

The Use of Multiquadric Radial Basis Functions in Open Region Problems

Richard K. Gordon and W. Elliott Hutchcraft

Department of Electrical Engineering
University of Mississippi
University, MS 38677

Email: eeqordon@olemiss.edu, eweh@olemiss.edu

Abstract — With the advent of neural networks, there has been a significant amount of research utilizing radial basis functions. In this paper, radial basis functions in conjunction with a meshless algorithm are used to solve electromagnetics problems in both open and closed regions. The algorithm for the solution of partial differential equations using the radial basis functions and development of the absorbing boundary condition will be discussed in detail. Several example problems will be discussed.

Keywords — radial basis functions, meshless algorithms, absorbing boundary conditions, partial differential equation techniques

I. INTRODUCTION

Radial basis functions (RBF) have received significant attention in the scientific literature over the past several years. Specifically, they have been investigated heavily in the field of neural networks. Until rather recently, RBF's have not been widely used in computational electromagnetics. They have been shown to have very good interpolation qualities and this has led to their recent use in inverse scattering methods in electromagnetics [1-11]. In this paper, radial basis functions in conjunction with a meshless algorithm are used to solve electromagnetics problems in both open and closed regions. In the next section, a discussion of the method used to solve partial

differential equations (PDE) using RBF's will be presented and an example will be shown. In Section III, the development of an absorbing boundary condition (ABC) based on the Wilcox expansion of the electric field will be presented and results utilizing the ABC will be shown. Finally, section IV will conclude the paper with discussions of some of the advantages and disadvantages of the proposed method.

II. SOLUTION OF PARTIAL DIFFERENTIAL EQUATIONS USING RADIAL BASIS FUNCTIONS

There are several different RBF's that could be used to solve PDEs, but in this paper, the focus will be on the multiquadric functions. These functions have a function representation of

$$\sqrt{1 + \frac{\|x - x_j\|^2}{c_j^2}}. \quad (1)$$

These functions have several interesting properties. The function's magnitude depends primarily upon the radial distance from its central location, x_j . This results in each slice of the function having a circular cross-section. In addition, these functions are continuous and have an infinite number of continuous derivatives at all points in space.

The algorithm employed in solving the PDEs in this research is termed a "meshless" method. This term is derived from the fact that

only information about nodes has to be known; in other words, no connectivity data between nodes is required. This is in contrast to the finite element method (FEM), which requires the knowledge of how the nodes are connected into elements. Generating a mesh for a detailed problem can be quite cumbersome and a misconnected node, which can easily go unnoticed, could lead to major problems. Obviously, since this is not necessary in this meshless algorithm, some of the problems associated with meshing can be alleviated. To discuss the details of the proposed algorithm, consider the closed region problem described by

$$\begin{aligned} \nabla^2 E_z + k^2 E_z &= 0 \quad \text{for } (x, y) \in \Omega \\ E_z(x, y) &= f(x, y) \quad \text{for } (x, y) \in \partial\Omega. \end{aligned} \quad (2)$$

The problem domain along with the associated boundary conditions is illustrated in Fig. 1. The radial basis functions will be used as the expansion for the electric field such that

$$E_z = \sum_{j=1}^N u_j \sqrt{1 + \frac{(x-x_j)^2 + (y-y_j)^2}{c_j^2}}. \quad (3)$$

$$\begin{aligned} E_z(x, 1.0) &= \sin\left(\frac{3\pi x}{a}\right) \\ E_z(0.0, y) &= 0.0 \quad \varepsilon \quad E_z(2.0, y) = 0.0 \\ E_z(x, 0.0) &= 0.0 \end{aligned}$$

Fig. 1. Closed region problem domain.

Here, the u_j 's are the unknown coefficients. The factor, c_j , is a scale factor for each RBF. In this research, all of the c_j 's have been chosen to be equal to 0.25. Now, the expansion (3) can be substituted into the original PDE (2) to obtain

$$\begin{aligned} \nabla^2 \left[\sum_{j=1}^N u_j \sqrt{1 + \frac{(x-x_j)^2 + (y-y_j)^2}{c_j^2}} \right] + \\ k^2 \sum_{j=1}^N u_j \sqrt{1 + \frac{(x-x_j)^2 + (y-y_j)^2}{c_j^2}} = 0. \end{aligned} \quad (4)$$

At this point, there are N unknown coefficients (the u_j 's) and only one equation. N equations are necessary to solve for the N u_j 's. The method used to obtain the N equations is called collocation. Collocation enforces either (4), or the boundary conditions, at the central points of the N RBF's. This yields a matrix equation

$$Mu = b \quad (5)$$

in which the matrix, M , will have elements

$$M_{i,j} = \begin{bmatrix} \nabla^2 \sqrt{1 + \frac{(x_i-x_j)^2 + (y_i-y_j)^2}{c_j^2}} \\ +k^2 \sqrt{1 + \frac{(x_i-x_j)^2 + (y_i-y_j)^2}{c_j^2}} \end{bmatrix} \text{ for } (x_i, y_i) \text{ in } \Omega \quad (6)$$

or

$$M_{i,j} = \sqrt{1 + \frac{(x_i-x_j)^2 + (y_i-y_j)^2}{c_j^2}} \text{ for } (x_i, y_i) \text{ on } \partial\Omega. \quad (7)$$

The right-hand side vector will have elements

$$b_j = \begin{cases} 0 & \text{for } (x_i, y_i) \text{ in } \Omega \\ f(x_i, y_i) & \text{for } (x_i, y_i) \text{ on } \partial\Omega \end{cases} \quad (8)$$

and the column vector, u , will be the vector containing the coefficients for the RBF's.

To illustrate that accurate results can be obtained for the aforementioned problem, consider the case for which $\varepsilon = 25.0$ and $\lambda = \frac{2\pi}{k} = 1.0$. Plots of both the numerical and analytic solution along the line $y = 0.3$ (Fig. 2) and $x = 0.5$ (Fig. 3) illustrate the accuracy that can be obtained using this method.

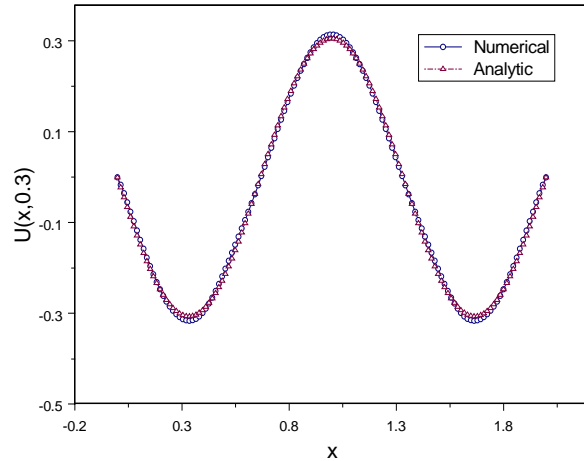


Fig. 2. Comparison of analytic and numerical solution (999 RBF's) along $y = 0$.

The solutions are obtained by employing 999 RBF's (33 equally spaced nodes along the x -direction and 33 equally spaced nodes along the y -direction) in the algorithm. In both cases, the numerical solutions lie nearly on top of the analytic solution.

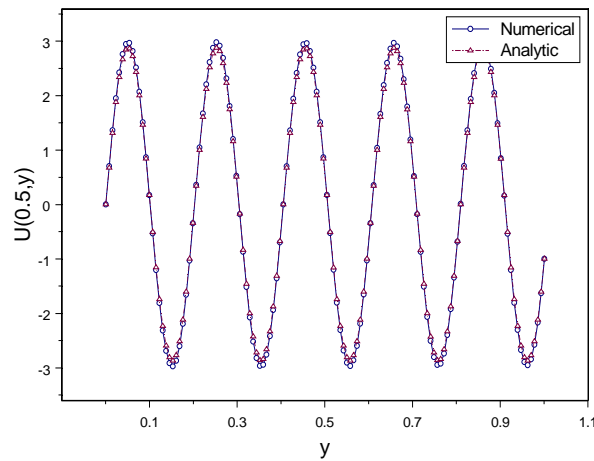


Fig. 3. Comparison of analytic and numerical solution (999 RBF's) along $x=0.5$.

This is rather impressive considering that there are only 33 basis functions in the y -direction and there are 5 wavelengths of variation in the y -direction. An investigation of the RMS Error as the number of RBF's is varied is shown in Fig.4.

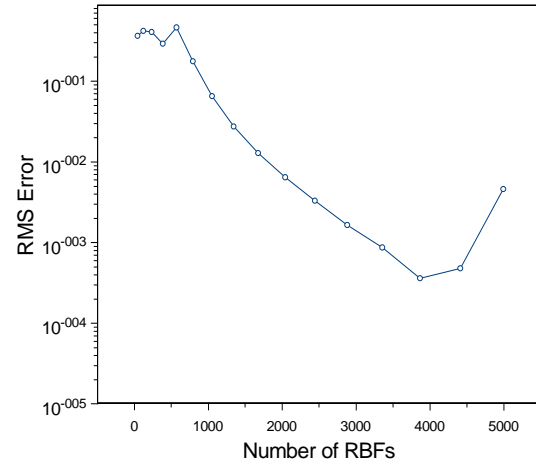


Fig. 4. RMS error as number of RBF's is varied.

This graph shows primarily what is expected. That is, as the number of RBF's is increased, the solution converges and the RMS error decreases. It should be pointed out that the computational cost of solving the matrix is higher than the traditional FEM for example, since the resulting matrix for this method is a full matrix. A direct solution technique (Gaussian elimination) was employed in the solution of the matrix equation. In addition to the disadvantage of having a full system matrix, the use of RBF's can result in ill-conditioning as the number of functions is increased. Ill-conditioning is primarily the problem for the increase in RMS error as the number of RBF's increases over 1000. A plot of the condition number as the number of RBF's is varied is shown in Fig. 5. It is important to realize that this graph is plotted on log axis; so, there are nearly 18 orders of magnitude difference between the smallest condition number and the largest condition number.

Further investigation of the condition number is required and some techniques to help alleviate the ill-conditioning will be presented in a separate paper. After seeing these results, though, it is clear that the RBF's

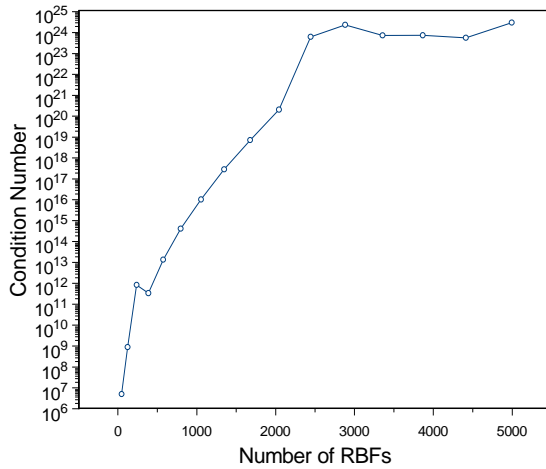


Fig. 5. Condition number as number of RBF's is varied.

can be used to solve closed region problems. In the next section, the focus will turn to that of the primary topic for this paper; that is, the discussion of the development of an ABC for an open region problem will be presented and then the ABC will be verified through several examples.

III. DEVELOPMENT OF AN ABSORBING BOUNDARY CONDITION FOR USE WITH RADIAL BASIS FUNCTIONS

Consider the scattering of a transverse magnetic (TM) incident plane wave on a cylinder of radius one wavelength as shown in Fig. 6. The nodes (central points) for the RBF's will be placed in the shaded region and along the inner and outer boundaries. The outer boundary will be placed 1.35 wavelengths away from the center of the perfect electrically conducting (PEC) cylinder. The equation enforced at collocation points that are between the PEC cylinder and the outer boundary is the Helmholtz equation

$$\nabla^2 E_z + k^2 E_z = 0. \quad (9)$$

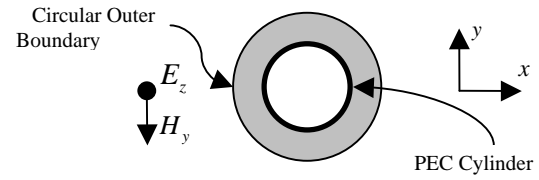


Fig. 6. Problem domain for circular PEC cylinder with circular outer boundary.

For collocation points that are on the circular cylinder, the equation enforced is

$$E_z = 0 \text{ for } r_i = \lambda \quad (10)$$

and for nodes along the outer boundary, the equation enforced will be

$$E_z(1.35, \phi) = AE_z(1.30, \phi) + BE_z(1.25, \phi). \quad (11)$$

There are several aspects that should be pointed out with respect to the implementation of the ABC. Equation (11) states that the electric field at the outer boundary is proportional to the electric field at two points that lie along the same phi plane and are 0.05 and 0.1 wavelengths interior to the outer boundary. The fact that $E_z(1.25, \phi)$ and $E_z(1.30, \phi)$ need to be known does not mean that nodes have to be placed at these locations. Since the RBF's are entire domain basis functions, a representation of E_z in terms of all of the RBF's can easily be found everywhere in the domain. Therefore, nodes are not necessary at $E_z(1.25, \phi)$ and $E_z(1.30, \phi)$. Obviously, the constants A and B in (11) must be obtained. It is first assumed that $E_z(1.25, \phi)$ and $E_z(1.30, \phi)$ can be approximated by the first two terms of the Wilcox expansion, which is

$$E_z(r, \phi) = \frac{e^{-jkr}}{\sqrt{r}} \left(C_1(\phi) + \frac{C_2(\phi)}{\rho} \right). \quad (12)$$

This assumption allows us to find C_1 and C_2 in terms of $E_z(1.25, \phi)$ and $E_z(1.30, \phi)$. Then, once these constants are known, the constants A and B can be found. After obtaining A and B , an expression for E_z along the outer boundary is known in terms of E_z at points slightly interior to the boundary. Now, by using equations (9), (10), and (11), a matrix equation can be formed and the coefficients for the RBF's can be obtained. The algorithm will initially be tested using 2636 RBF's. Since the region between the cylinder and the outer boundary has an area equal to 2.5 square wavelengths, this problem domain has been discretized to yield approximately 32 functions/wavelength. In Figs. 7 and 8, the numerical and analytic solutions for the magnitude and the phase of the electric surface current on the PEC cylinder are compared. With this mesh density, a nodal average percent error was calculated to be 1.46%.

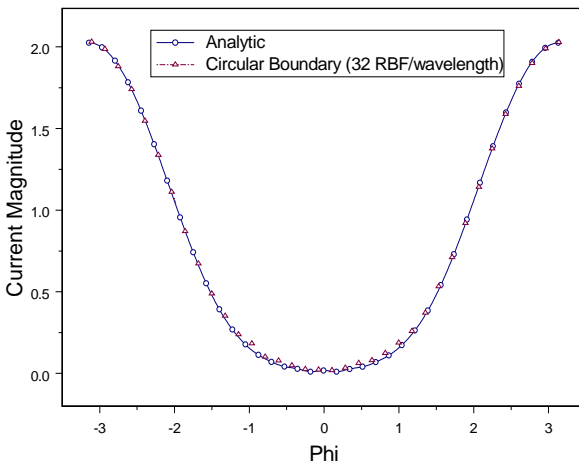


Fig. 7. Magnitude of the current along the cylinder (~ 32 RBF/wavelength).

Since 32 functions/wavelength is a rather high mesh density, the results of a simulation in which the mesh density was lowered to approximately 23 functions/wavelength (1416 nodes) are presented in Figs. 9 and 10. Even at this density, the average percentage error was still very low at only 1.6%. At this point,

the ABC has been verified to work properly for a circular outer boundary.

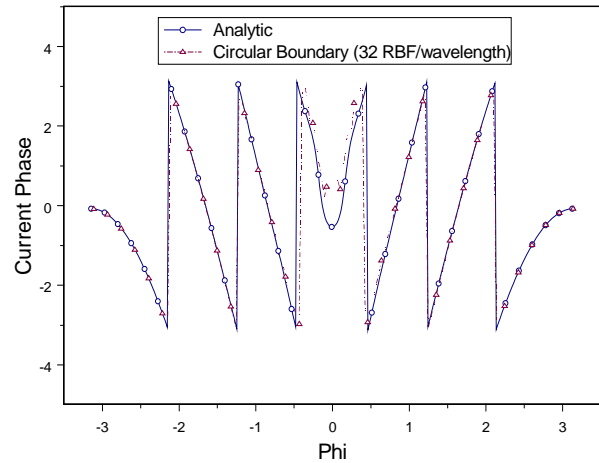


Fig. 8. Phase of the current along the cylinder (~ 32 RBF/wavelength).

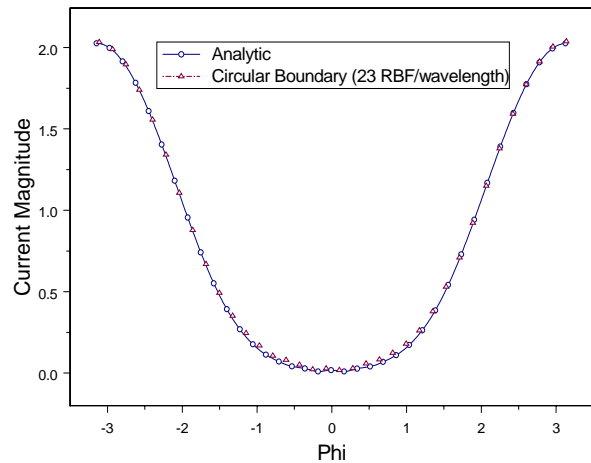


Fig. 9. Magnitude of the current along the cylinder (~ 23 RBF/wavelength).

However, one of the problems often encountered with ABCs is that special meshing is required at the boundary so that the ABC can be implemented. For example, this could include placing the nodes close to the edge of the outer boundary along a constant phi plane or having a circular boundary, etc. To illustrate the robustness of the developed ABC and show that it does not have this requirement, the same cylinder will be

considered, but the outer boundary will be changed from a circular outer boundary to a square outer boundary. An illustration of the problem domain is shown in Fig. 11.

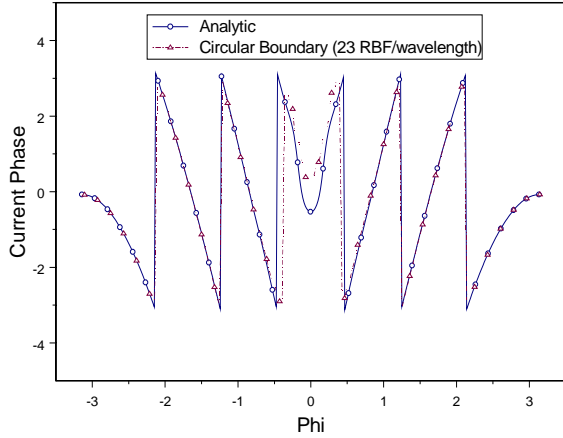


Fig. 10. Phase of the current along the cylinder (~23 RBF/wavelength).

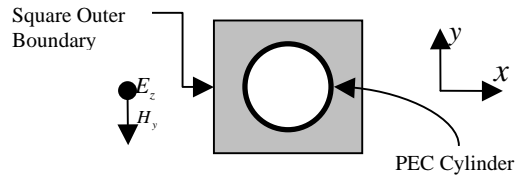


Fig. 11. Problem domain for circular PEC cylinder with circular outer boundary.

The center of each side of the square boundary will be tangent to the circular boundary from the previous example. Thus, the square’s sides will have lengths of 2.7 wavelengths and the region between the cylinder and outer boundary will have an area equal to 4.15 square wavelengths. A total of 2512 RBF’s were used in the simulation. This resulted in a mesh density of approximately 25 functions / wavelength. Comparisons of the numerical and analytic solutions for the magnitude and phase are presented in Figs. 12 and 13, respectively. The average percent error per node was 2.08%. From these graphs, one can conclude that switching from a

circular outer boundary to a square outer boundary did not significantly affect the results. This is particularly beneficial since it is desired to keep this method a “meshless” algorithm. We do not want to have to be very specific about where to put the RBF’s in the problem domain and we also do not want to specify a specific type of outer boundary.

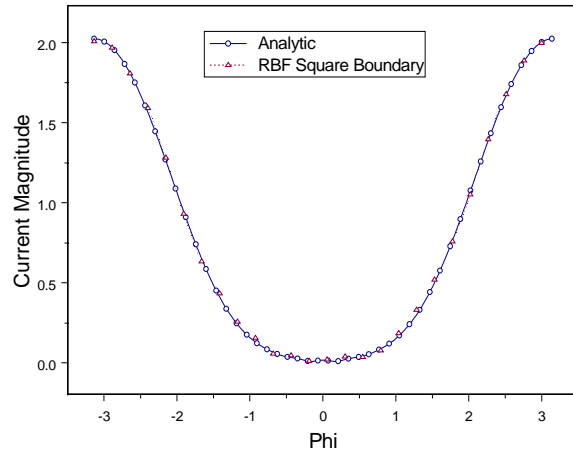


Fig. 12. Magnitude of the current along the cylinder (~25 RBF/wavelength) with square boundary.

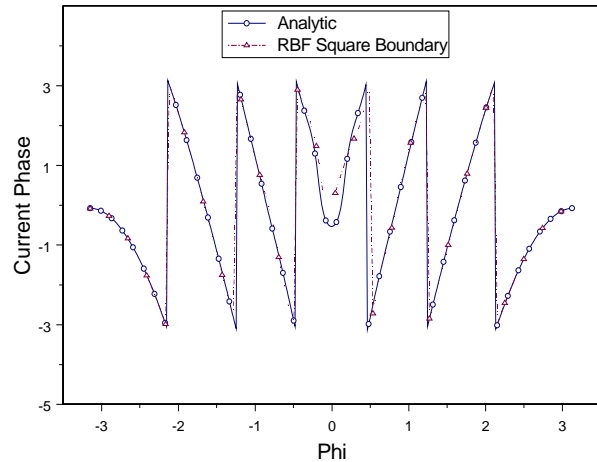


Fig. 13. Phase of the current along the cylinder (~25 RBF/wavelength) with square boundary.

IV. CONCLUSION

We have shown in this research a proof-of-

concept that a meshless method employing multiquadric radial basis functions and collocation can be used to obtain accurate results for both closed region and open region problems. Among the principle advantages of this method are the simplicity of the programming and the elimination of the need for sophisticated meshing. Among the disadvantages of this method is the fact that it yields a full matrix and that matrix can be ill-conditioned as the number of RBF's is increased. This problem is alleviated somewhat by the quickness of which each matrix element can be obtained. In addition, ill-conditioning can also result if care is not taken. Future research includes an investigation of the condition number and ways to prevent and alleviate the ill-conditioning problem that can result. Included in this investigation will be an investigation of node placement strategies as well as choice of the shape factor (c_{val}); in addition, future work will also investigate what happens with discontinuities in the problem domain and how they should be handled.

REFERENCES

- [1] M. J. F. A. I. Fedoseyev, E. J. Kansa, "Continuation for Nonlinear Elliptic Partial Differential Equations Discretized By The Multiquadric Method," *International Journal of Bifurcation and Chaos*, vol. 10, pp. 481-491, 2000.
- [2] S. C. E. Bermani, M. Raffetto, "A Threshold Electromagnetic classification approach for cylinders embedded in a lossy medium by using a neural network technique," *Microwave Opt. Technol Let*, vol. 24, pp. 13-16, 2000.
- [3] S. C. E. Bermani, M. Raffetto, "Microwave detection and dielectric characterization of cylindrical objects from amplitude-only data by means of neural networks," *IEEE Trans Antennas Propagat*, vol. 50, pp. 1309-1314, 2002.
- [4] L. U. I. Elshafiey, S. S. Udpa, "Solution of inverse problems in electromagnetics using hopfield neural networks," *IEEE Trans Magn*, vol. 31, pp. 852-861, 1995.
- [5] W. Y. Liu Guosui, Yang Chunling, Zhou Dequan, "Radar Target Classification Based on Radial Basis Function and Modified Radial Basis Function Networks," pp. 208-211.
- [6] K. A. M. R. Mydur, "A Neural-Network Approach to the Electromagnetic Imaging of Elliptic Conducting Cylinders," *Microwave Opt. Technol Let*, vol. 28, pp. 303-306, 2001.
- [7] I. T. Rekanos, "On-line inverse scattering of conducting cylinders using radial basis-function neural networks," *Microwave Opt. Technol Let*, vol. 28, pp. 378-380, 2001.
- [8] I. T. Rekanos, "Neural-network-based inverse-scattering technique for online microwave medical imaging," *IEEE Trans Magn*, vol. 38, pp. 1061-1064, 2002.
- [9] P. G. S. Caorsi, "Electromagnetic Detection of Dielectric Cylinders by a Neural Network Approach," *IEEE Trans Geosci Remote Sensing*, vol. 37, pp. 820-827, 1999.
- [10] H. H. S. Ratnajeevan, "Artificial Neural Networks in the Solution of Inverse Electromagnetic Field Problems," *IEEE Trans Magn*, vol. 29, pp. 1931-1934, 1993.
- [11] F. N. C. S. Chen, P. M. Grant, "Orthogonal least squares learning algorithm for radial basis function networks," *IEEE Trans Neural Networks*, vol. 2, pp. 302-309, 1991.



Richard K. Gordon was born in Birmingham, Alabama on November 26, 1959. He earned his B.S. in physics at Birmingham Southern College, Birmingham, AL in 1983, his M.S. in mathematics at the University of Illinois,

Urbana, IL in 1986 and his Ph. D. in electrical engineering at the University of Illinois, Urbana, IL in 1990.

He is an Associate Professor in the Department of Electrical Engineering at the University of Mississippi in Oxford, Mississippi.

Dr. Gordon is a member of Eta Kappa Nu, Phi Beta Kappa, and Tau Beta Pi.



W. Elliott Hutchcraft was born in Lexington, Kentucky on April 29, 1973. He earned his B.S. in electrical engineering at the University of Mississippi, Oxford, MS in 1996, his M.S. in electrical engineering at the

University of Mississippi, Oxford, MS in 1998 and his Ph. D. in electrical engineering at the University of Mississippi, Oxford, MS in 2003.

He is an Assistant Professor in the Department of Electrical Engineering at the University of Mississippi in Oxford, Mississippi.

Dr. Hutchcraft is a member of Eta Kappa Nu, Sigma Xi, IEEE, Tau Beta Pi, Phi Kappa Phi, and ARFTG.